Effect of Oxide Film Properties on the Kinetics of O_2 Reduction on Alloy C-22

Xiangrong Zhang,[a] Zack Qin,[a] Dmitrij Zagidulin,[a] James J. Noël,[a,b,*,z] and David W. Shoesmith[a,b,,z]**

[a]*Department of Chemistry, University of Western Ontario, London, Ontario N6A 5B7, Canada*
[b]*Surface Science Western, University of Western Ontario, London, Ontario N6G 0J3, Canada*

The kinetics of oxygen reduction have been studied electrochemically on the Ni-Cr-Mo(W) Alloy C-22 in 5 M NaCl at 70°C using potentiostatic and voltammetric techniques and electrochemical impedance spectroscopy. Oxygen reduction was observed to occur at low potentials on defective oxide films containing a high concentration of anion vacancies and appeared to proceed by a combination of 2-electron and 4-electron transfer processes. At more positive potentials a passive film comprising a Cr^{III}-dominated barrier layer at the alloy/oxide interface and a Mo/W enriched outer layer at the oxide/solution interface was formed, and oxygen reduction was completely suppressed. Oxygen reduction could be revived after transpassive degradation of the oxide film at more positive potentials, and appeared to be catalyzed on the Mo^{VI}/W^{VI} surface film.

Manuscript submitted July 3, 2017; revised manuscript received October 23, 2017. Published November 8, 2017.

Ni-Cr-Mo alloys are well known high-performance alloys that exhibit exceptional corrosion resistance under extreme exposure conditions. These alloys are widely used by chemical processing industries, and in the areas of energy, health and environmental applications, oil, gas and pharmaceuticals.

A primary asset of Ni-Cr-Mo alloys is their ability to withstand localized corrosion processes, such as pitting, crevice corrosion, intergranular corrosion, and stress corrosion cracking. Their reliable performance under extreme industrial conditions is generally attributed to their elemental composition and the passive behavior it induces. A wide array of in-situ and ex-situ analytical techniques[1–8] has been employed to assess passive behavior and its influence on the corrosion performance of these alloys. The combination of high Cr and Mo contents leads to the formation of a Cr-dominated passive oxide film[2,3,9–11] with a duplex film structure,[12] which provides resistance against oxidizing environments.[13] The nature and composition of these oxide films depend on alloy composition, potential, pH, temperature, and the composition of the environment in which they are formed.

If these alloys are to suffer localized corrosion, the most likely form appears to be crevice corrosion,[14–21] and the accumulation of localized corrosion damage would require metal dissolution inside a creviced area to be supported by the cathodic reduction of O_2 on oxide-covered surfaces outside the crevice, although internal support by proton reduction has also recently been observed.[21] This makes knowledge of the kinetics for O_2 reduction essential for the development of corrosion models.[22] Despite its importance, the kinetics of this reaction have not been extensively studied on oxide-covered Ni-Cr-Mo alloys.

The influence of passive films on O_2 reduction kinetics is known to be complex.[23] In aqueous (neutral to alkaline) solutions, the cathodic reduction of O_2 proceeds via a direct 4-electron transfer process,[23]

$$O_2 + 2H_2O + 4e^- \rightarrow 4OH^- \quad [1]$$

or two consecutive 2-electron transfer processes involving the intermediate production of H_2O_2,

$$O_2 + 2H_2O + 2e^- \rightarrow H_2O_2 + 2OH^- \quad [2]$$

$$H_2O_2 + 2e^- \rightarrow 2OH^- \quad [3]$$

A parallel pathway involving both processes has also been demonstrated.[23]

The reduction pathway is influenced by many factors. On passive Fe, Ni, and stainless steel, the current for O_2 reduction exhibits a pH dependence attributed to the n-type semiconducting nature of the passive film.[24] The kinetics are also affected by electrode surface treatment.[25] For example, the O_2 reduction rate on stainless steels increases in the order: chemically treated surface (with HF/HNO_3) < anodically passivated surface < mechanically polished surface (with a 1 μm Al_2O_3 suspension) < cathodically pre-reduced surface (–1.055 V (vs. sat. Ag/AgCl) for 10 min). On cathodically pre-reduced and polished surfaces, O_2 reduction is mass transport-limited. On passivated surfaces, the currents are lower, due either to a limited access of O_2 to the metal surface or to the modified electronic conductivity of the oxide, and reduction is effectively suppressed on chemically treated surfaces.

On pre-reduced surfaces, reduction occurs via the 4-electron pathway (Reaction 1), while on polished surfaces a parallel mechanism is involved. The mechanism of O_2 reduction on the passivated surface has not been identified, although the mechanism is found to differ between bare Fe and passive Fe in neutral solutions.[26] On bare Fe, the reaction proceeds via the 4-electron pathway with little H_2O_2 formed as an intermediate, and the formation of the superoxide radical being the rate-determining step. By contrast, on passive Fe, reduction proceeds through a 2-electron pathway, yielding H_2O_2, with the chemisorption of O_2 proposed as the rate-determining step. The rate of O_2 reduction on passive Fe is greater than that on bare Fe, due to a strong catalytic effect of the passive iron oxide film.[26]

The O_2 reduction reaction on Alloys C-22 and C-276 in alkaline solutions appears to proceed via two 2-electron processes in series, with kinetic rate constants at 30°C estimated to be in the range 0.001 to 0.232 cm/s, depending on the potential.[27] An electrochemical and corrosion study of Alloy C-22 in 0.5 M NaCl solution showed that open-circuit passivation of the alloy had a pronounced effect on the kinetic parameters of both the cathodic and anodic reactions involved in the corrosion process.[28] Both reactions were slower than those proceeding on the active (cathodically-reduced) alloy surface. On this latter surface, a limiting current for a 4-electron reduction of O_2 was observed, and an apparent Tafel slope in the range –50 to –70 mV/decade obtained. However, after 3 h on open circuit, the slope increased to a value in the range –115 to –175 mV/decade, and no limiting current was observed.[28]

On an Alloy C-22 surface claimed to be free of oxide, the kinetics have been explored over wide ranges of pH and temperature.[22] A diffusion limited current was found for large negative potentials at

*Electrochemical Society Member.
**Electrochemical Society Fellow.
[z]E-mail: jjnoel@uwo.ca; dwshoesm@uwo.ca

pH ≥ 4. The limiting current density increased over the temperature range from 20°C to 70°C, but decreased with a further temperature increase to 95°C. This was attributed to competition between an increase in the mass transfer rate and a decrease in O_2 solubility in the bulk electrolyte at high temperatures. A dual-wave polarization curve indicating two consecutive two-electron transfer processes and the formation of the intermediate, H_2O_2, was observed only at 70 and 95°C. As expected, the limiting current density also depended linearly on the dissolved [O_2], and was virtually independent of solution pH in the range of 4 ≤ pH ≤ 8. An increase in [O_2] also resulted in higher E_{corr} values and corrosion rates of Alloy 625 in ammoniacal sulfate solution from 25 to 200°C.[29] The O_2 reduction current became increasingly diffusion controlled as temperature and O_2 partial pressure were increased, reportedly as the oxide barrier layer thickness and resistance decreased with temperature.

None of these studies attempted to characterize in detail the influence of oxide film properties on O_2 reduction kinetics. We have previously characterized the evolution of film composition as a function of potential on Alloy C-22 (Ni-23Cr-13Mo-3W-3Fe)[30] and as a function of potential and temperature on Alloy C-2000 (Ni-23Cr-16Mo-1.6Cu).[31,32] In this study, the kinetics of O_2 reduction have been studied using a range of electrochemical techniques. Potentiostatic polarizations and cyclic voltammetry were performed in both oxygenated and deoxygenated 5 M NaCl solutions over different potential ranges, including both the passive and transpassive regions at 70°C. Oxide films were grown at different potentials throughout the passive and transpassive potential regions and their properties characterized using electrochemical impedance spectroscopy (EIS).

Experimental

Electrochemical cell and solution.—A three-electrode electrochemical cell with a Pt (99.95% purity) counter electrode and an in-house fabricated Ag/AgCl reference electrode (RE) in saturated KCl solution (199 mV vs. SHE at 25°C) were used in all experiments. All potential values are reported against the saturated Ag/AgCl electrode. The cell was fitted with an outer jacket through which silicon oil or deionized water was circulated from a thermostatic bath (Isotemp 3016H, Fisher Scientific) to maintain the temperature of the solution to within ±1°C. To avoid extraneous electrical noise the cell was housed in a grounded Faraday cage. Experiments were performed at 70°C. A rotating disc working electrode setup was used at a rotation rate of 1400 rpm in all electrochemical experiments except for EIS measurements.

5 M NaCl solutions were prepared from reagent grade NaCl and Type-I water (resistivity of 18.2 MΩ · cm, obtained from a Milli-Q Academic A-10 system). Prior to each experiment, the solution was sparged for at least 1 h with either Grade 4.4 O_2 or UHP Ar (Praxair) with sparging continued throughout the experiment. For Ar-sparged experiments we estimate that the residual dissolved [O_2] was 0.2 to 0.4 ppm.[33] The solutions were maintained at pH 7 by adding 0.1 M HCl and NaOH solutions as necessary.

Materials and electrode preparation.—Working electrodes (WE) were cut as cylinders (diameter 1 cm, with thickness 0.5 to 1 cm) from plate materials supplied by Haynes International, Kokomo, Indiana (USA). Electrodes were encased in a heat-resistant epoxy resin (Dexter Hysol resin EE4183, hardener HD3561) with only a single flat face (with a surface area of 0.785 cm^2) exposed to the solution. Before each experiment, the electrode was wet ground sequentially with a series of SiC papers up to 1200 grit, ultrasonically cleaned for 10 minutes, first in methanol and then in Type-I water, and then immediately placed in the cell.

Specimens in experiments involving surface analyses were polished successively with alumina powder suspensions to a 0.05 μm finish, rinsed with copious amounts of Type-I water, ultrasonically cleaned for 10 minutes in methanol, and then finally rinsed in Type-I water.

Electrochemical procedure.—All experiments were performed with a Solartron 1287 potentiostat and a Solartron 1255 frequency response analyzer (FRA). Electrodes were rotated using an analytical rotator (Pine Instruments) with an ASR speed control. CorrWare and ZPlot software (for EIS) (Scribner Associates) were used to record and analyze data. All the electrochemical experiments were repeated at least three times and the average values were used.

In electrochemical experiments the electrode was cathodically cleaned at –1.0 V for 1 h. Such a treatment has been shown to produce a highly defective oxide.[34] The potential was then increased in 0.1 V increments from this potential to the chosen anodic potential limit (positive scan) and then decreased in similar steps back to –0.9 V (negative scan). The potential was held at each value for 1 h. The current at the end of this period was used to plot polarization curves. Before EIS measurements the potential was held for 2 h. EIS experiments were performed using a sinusoidal input potential with an amplitude of ± 10 mV at eleven individual frequencies over the range 100 kHz to 0.005 Hz. The self-consistency of the measured spectra was tested using the Kramers–Kronig transformation.[35,36]

In cyclic voltammetry (CV) experiments, after a period of cathodic cleaning, the potential was scanned to a specific film-growth potential at 5 mV/s, held at this value (between –0.6 V and 0.6 V) for 1 h to allow film growth, and then scanned to –1 V (negative scan) and back to the film-growth potential (positive scan) at 5 mV/s.

Results

Corrosion potential.—In an oxygenated solution, the corrosion potential (E_{corr}) rapidly increased after cathodic cleaning to a steady-state value of ∼ −0.15 V. In an Ar-purged solution, E_{corr} increased more slowly to a value in the range −0.4 V to −0.5 V (4 h) and then steadily increased to ∼ −0.35 V after 24 h. The latter increase can be attributed to slow oxidation of the surface by the residual traces of dissolved O_2 in the Ar-purged solution and the slow self-repair of defects in the passive layer.

Potentiostatic polarization at 70°C.—Figure 1a shows the steady-state polarization curves recorded in oxygenated solutions at 70°C for both increasing (positive-going scan) and decreasing (negative-going scan) potentials. On the positive-going scan three distinct regions, but no active region, were observed: (i) a region (1) within which O_2 reduction is observed as a shoulder in the potential range ∼ −0.8 V to −0.4 V on the more prominent current increase observed for H_2O reduction in this region; (ii) a region (2) in which the current density is small (<1 $\mu A \cdot cm^{-2}$) and independent of applied potential, over the potential range from ∼ −0.2 V to ∼ 0.4 V, with the lower limit being defined by the potential at which O_2 reduction becomes undetectable and the upper limit by the eventual increase in current; and (iii) region (3) which commences at the potential at which the current begins to increase at the end of region (2).

These regions, and the characteristics of the surface films present, have been investigated previously on a number of Ni-Cr and Ni-Cr-Mo alloys.[1,30] In region (1) the oxide film present on the alloy surface was shown to be highly defective due to the presence of a large concentration of anion vacancies.[37–39] In region (2), a Cr^{III} oxide barrier layer developed and thickened as the potential was increased, accompanied by the segregation of Mo, and to a lesser degree W, to the outer regions of the film.[1,31] In region (3) (the transpassive region) this barrier layer was degraded as Cr^{III} was oxidized to the more soluble Cr^{VI}, and the film thickened due to the accumulation of Mo^{VI}/W^{VI} species at the oxide /solution interface.[1,2,30,31]

The current observed on the negative-going scan depended on the potential limit of the preceding positive-going scan. The O_2 reduction current was larger if the potential had been scanned into the transpassive region, region 3 (0.9 V), than if the scan was reversed in the passive region (0.1 V), Figure 1b. The extremely small O_2 reduction current observed when the polarization curve was recorded from an anodic limit of 0.1 V indicated that the reaction was effectively suppressed by formation of the passive film. The larger reduction current

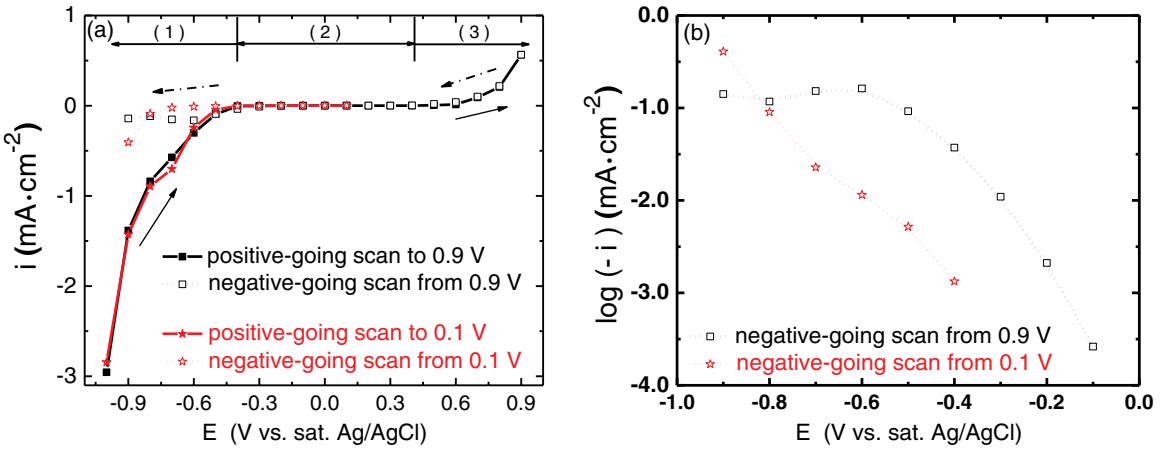

Figure 1. (a) Potentiostatic polarization curves recorded on Alloy C-22 in oxygenated 5 M NaCl solution (pH = 7) at 70°C at electrode rotation rate of 1400 rpm; (b) cathodic O_2 and H_2O reduction current densities obtained on the negative scans.

density observed after the potential was extended to 0.9 V showed that O_2 reduction was revived to some degree on the surface after reactivation in the transpassive region.

The differences between the polarization curves recorded up to 0.9 V in deoxygenated and oxygenated solutions, Figure 2a, enabled the net O_2 reduction current densities (i) to be determined, Figure 2b. A linear relationship between log (– i) and E was obtained on the positive-going scan in the potential region −0.6 V to −0.2 V, suggesting Tafel behavior, as illustrated by the green line. The slope was calculated to be 118 ± 10 mV/decade compared to a theoretical value of 136 mV/decade assuming rate control by the first electron transfer (with the transfer coefficient taken to be 0.5).

After polarization of the electrode to 0.9 V, the O_2 reduction current was enhanced at potentials in the range (−0.2 to −0.5 V) compared to the currents measured on the positive-going scan, Figure 2b. This suggests either catalysis of the first electron transfer rate-controlling process by the Mo (or W) species at high oxidation states, which are formed and accumulate on the surface in the transpassive region, or easier electron transfer through the partially destroyed barrier layer of the film, which is not completely repaired on the negative-going scan. Also, the shape of the polarization curve changes markedly. The current was not linearly related to E as observed on the positive-going scan, the current rising more rapidly with potential to a maximum at −0.6 V before decreasing as the potential was further decreased. A possibility was that the catalytic Mo (W) states accounted for the steep increase in current density but were destroyed electrochemically at more negative potentials, leading to the decrease in the O_2 reduction current density.

The single current plateau, with a limiting current density of ~0.63 mA/cm^2 (for potentials between –1.0 V and –0.6 V), observed on the positive-going scan for O_2 reduction, Figure 2b, was consistent with the literature.[29] The theoretical limiting cathodic currents (i_L) expected for either a 2- or a 4-electron process, Reactions 1 and 2, respectively, can be calculated using the Levich Equation[40]

$$i_L = 0.620nFAD^{2/3}\omega^{1/2}\upsilon^{-1/6}c^b \quad [4]$$

using an electrode surface area (A) of 0.785 cm^2 and a value of kinematic viscosity (υ) for 5 M NaCl of 6.367×10^{-2} cm$^2 \cdot$ s^{-1} obtained from the CRC handbook by assuming a constant viscosity ratio of 1.871 relative to water at the same temperature.[41–43] A value of the diffusion coefficient (D) for O_2 of 2.98×10^{-5} cm$^2 \cdot$ s^{-1} was calculated using the Stokes-Einstein equation

$$\frac{D\upsilon}{T} = \frac{k'}{6\pi r} = \text{constant} \quad [5]$$

and experimentally measured parameter values in water.[43–45] In Equation 5, T is the absolute temperature, k' is the Boltzmann constant, and r is the radius of the solute molecule. The bulk solution concentration of O_2 at 70°C in 5 M NaCl, c^b in Equation 4 or $(c_{aq})_l$ in Equation 6, was calculated to be 1.432×10^{-7} mol $\cdot$ cm^{-3} using

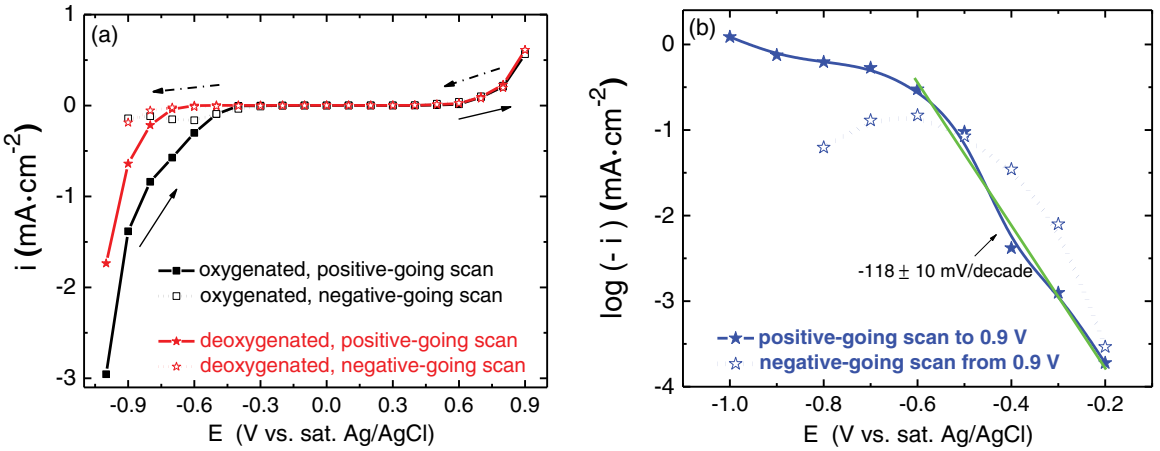

Figure 2. (a) Potentiostatic polarization curves recorded on Alloy C-22 in either oxygenated or deoxygenated 5 M NaCl (pH = 7) at 70°C at a rotation rate of 1400 rpm; (b) net O_2 reduction current after subtraction of the current for H_2O reduction recorded in deoxygenated solution. The green line is a least-squares fit to 5 points.

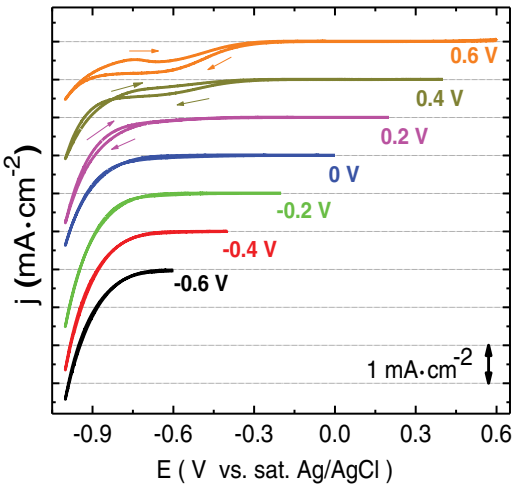

Figure 3. CVs recorded on Alloy C-22 after potentiostatic oxidation at various potentials for 1 h in oxygenated 5 M NaCl at 70°C at a rotation rate of 1400 rpm. The currents are shown offset by 1 mA · cm^{-2}. The potential scan rate was 5 mV · s^{-1}.

Equations 6 and 7 to predict O_2 solubility in an electrolyte solution[46]

$$\frac{(c_{aq})_l}{P_{O2}} = K\left(1 + \kappa c_l^{y}\right)^{-h} \quad [6]$$

where $(c_{aq})_l$ (mol · cm^{-3}) is the concentration of O_2 in the electrolyte; P_{O2} (atm) is the partial pressure of O_2, corrected for the vapor pressure of water at the same temperature; c_l (5 M) is the concentration of electrolyte; κ, y and h are empirical modeling parameters used to define the effect of inorganic solutes on O_2 solubility, with values 0.076, 1.01 and 4.224 for NaCl, respectively; and K is the equilibrium constant for the phase equilibrium between dissolved and gas phase O_2,[46] given by

$$K = \exp\left\{\frac{\left[0.046T^2 + 203.35T\ln\left(\frac{T}{298}\right) - (299.378 + 0.092T)(T - 298) - 20.591 \times 10^3\right]}{8.3144T}\right\} \quad [7]$$

The empirical parameters are evaluated from fits of (c_{aq}) to c_l using available electrolyte solubility data.

Based on this calculation, the theoretical limiting current densities for 2- and 4- electron O_2 reduction processes are 0.46 and 0.92 mA · cm^{-2}, respectively. Comparison to the experimental limiting current density of 0.63 mA · cm^{-2}, measured on a positive-going scan, suggests O_2 reduction on Alloy C-22 does not proceed via either a 2- or a 4-electron process, but possibly by a mixture of both. Alternatively, the reaction may be a 4-electron process that is partially suppressed on a defective oxide surface. The maximum current of 0.14 mA · cm^{-2} observed at –0.6 V on the negative-going scan (after polarization up to 0.9 V) indicates that O_2 reduction is eventually partially suppressed as the potential is made more negative on the re-activated surface, making it impossible to determine whether the reaction involves a 4-electron or a 2-electron process on this surface.

The effect of film-growth potential on the kinetics of O_2 reduction observed in this study was in agreement with the results in the literature[28] which showed that the self-passivation of Alloy C-22 had a pronounced effect on the kinetic parameters of both cathodic and anodic reactions of the corrosion process in a 0.5 M NaCl solution.

Potentiostatic film-growth followed by cyclic voltammetry at 70°C.—The kinetics of O_2 reduction were also investigated on the surfaces of Alloy C-22 oxidized at single potentials. After oxide film growth for 1 h at the selected potentials on a previously cathodically cleaned surface, the potential was scanned from the film-growth potential to a negative limit of −1 V (negative-going scan) and back (positive-going scan) at a scan rate of 5 mV · s^{-1}, Figure 3. In oxygenated solutions, reversible current-potential behavior was observed after oxidation at potentials of –0.6 and –0.4 V. While no distinct wave for O_2 reduction was observed, the cathodic currents were large, suggesting that neither O_2 nor H_2O reduction were totally suppressed within region 1 when a highly defective oxide was present. After oxidation in the passive region (0 V) the cathodic current was suppressed, indicating that O_2 reduction was completely inhibited on the passive oxide film, consistent with the potentiostatic polarization experiments in Potentiostatic polarization at 70°C section. After anodic oxidation at 0.2 V, a minor reduction current was observed, beginning just below −0.5 V. This small reduction current could have been due to O_2 reduction on a surface that was slightly reactivated by minor defect injection. The decreasing oxide film resistance and increasing oxide film capacitance observed at potentials above 0.2 V in the EIS results of Jakupi et al.[1] demonstrate that this is the potential beyond which film degradation leading to the onset of transpassivity becomes feasible.

After polarization in the transpassive region, region 3 (0.4 to 0.6 V), a very distinct O_2 reduction current density was observed on the negative-going scan, with the magnitude of the current density in the plateau region being greater after polarization at 0.6 V than after polarization at 0.4 V. This was consistent with the claim (above) that O_2 reduction can be catalyzed on the oxidized Mo and W species produced in the transpassive region. The higher O_2 reduction current density after polarization at 0.6 V would then reflect a more complete surface coverage with these species. This was expected since we have previously shown[31] that oxidation in the transpassive region does not occur uniformly on the electrode surface. This increase in current density after polarization at the higher potential was likely attributable to a more extensive coverage of the surface by catalytic Mo^{VI}/W^{VI} species. The lower O_2 reduction current density on the subsequent positive-going scan suggested the reduction (at least partially) of these species at more negative potentials. It is also worth noting that the current density due to H_2O reduction was significantly depressed at the negative potential limit.

A similar series of experiments in deoxygenated solutions, Figure 4, showed that transformations in the properties of the oxide also occurred. In anodic oxidations at potentials up to 0 V there was no indication that the properties of the oxide were changed by either the anodic oxidation or the subsequent negative and positive-going scans. However, once the potential was increased to ≥ 0.2 V, the threshold for film degradation leading to the onset of transpassivity,[1] a slight hysteresis on the negative-going scan and a re-oxidation peak on the subsequent positive-going scan were observed. If the potential limit was increased to 0.4 V or 0.6 V the re-oxidation process became more marked. Also, the current for H_2O reduction at very negative potentials (−0.9 V to −1.0 V) was suppressed after oxidation of the alloy in the transpassive region 3. Since these effects were not observed after oxidation in the passive region 2 they were clearly related to the destruction of the Cr^{III} oxide barrier layer and the formation of high oxidation states of Mo and W in the transpassive region 3.

EIS measurements at 70°C.—EIS were recorded after each 2-h anodic oxidation at a series of potentials starting from –1.0 V in both oxygenated and deoxygenated stagnant solutions at 70°C. Figure 5 shows Bode plots obtained at selected potentials on the positive- and negative-going scans of the polarization curve. Over the

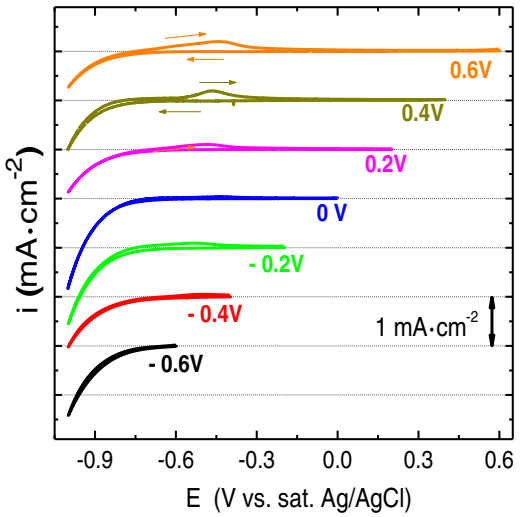

Figure 4. CVs recorded on Alloy C-22 after potentiostatic oxidation at various potentials for 1 h in deoxygenated 5 M NaCl at 70°C at a rotation rate of 1400 rpm. The currents are shown offset by 1 mA · cm^{-2}. The potential scan rate was 5 mV · s^{-1}

potential range –0.9 V to ~0.2 V, the magnitude of the low-frequency impedance (|*Z*|) increased with increasing potential (Figure 5a) before decreasing again as the potential was further increased up to 0.9 V. This was consistent with film thickening and the elimination of defects at potentials in the passive region 2 and with film degradation in region 3.

In experiments performed at intermediate potentials, the phase angle (θ) vs frequency plots (Figure 5b) exhibit two maxima at intermediate potentials (−0.5 V to 0.6 V), indicating the presence of two time constants. Though not shown here, only one maximum in the phase angle was observed at low (E ≤ – 0.6 V) and high (E ≥ 0.7 V) potentials, indicating the presence of only one time constant.

The solid curves in Figure 5 show how well the spectra can be fitted by the electrical equivalent circuits shown in Figure 6. For the positive-going scan, spectra recorded at the negative and positive ends of the potential range (E ≤ –0.6 V and E ≥ 0.7 V), regions 1 and 3, were fitted by a one time constant equivalent circuit, Figure 6a. The impedance response (R_1/CPE_1), which occurred between 10 and 10^3 Hz, was taken to represent charge transfer at the oxide/solution interface at low potentials in region 1 (as defined in Figure 1), i.e., charge transfer leading to O_2 and/or H_2O reduction at negative potentials. At high potentials in region 3 (as defined in Figure 1) this response was attributed to the creation of the high oxidation states of Mo and W. Spectra exhibiting two maxima in the phase angle plot were fitted by the equivalent circuit shown in Figure 6b, with the high frequency response attributed to charge transfer at the alloy/barrier layer oxide interface (R_1/CPE_1). The low frequency response, commonly observed in potential regions 2 and 3, was attributed to the properties of the passive and/or transpassive film (R_F/CPE_F).

In fitting the EIS data, constant phase elements (CPE) were used instead of capacitors to account for non-ideal capacitive behaviors attributed to time-constant dispersion. The impedance of a CPE is defined as

$$Z_{\mathrm{CPE}}(\omega) = [Y_0(j\omega)^n]^{-1} \quad (j^2 = -1) \qquad [8]$$

where ω is the angular frequency, Y_0 the CPE amplitude, and n the CPE exponent which is independent of ω. When the exponent n = 1, the CPE is identical to a capacitor. At intermediate values of n, the CPE is a phenomenological term with no simple physical justification. The common methods for the conversion of CPE parameters to C are those proposed by Brug[47,48] and by Hsu and Mansfeld.[49] However, it was not until recently that it was made clear that Hsu and Mansfeld's formula is applicable to time-constant dispersion normal to the surface, while that of Brug is applicable to surface dispersion.[47,48]

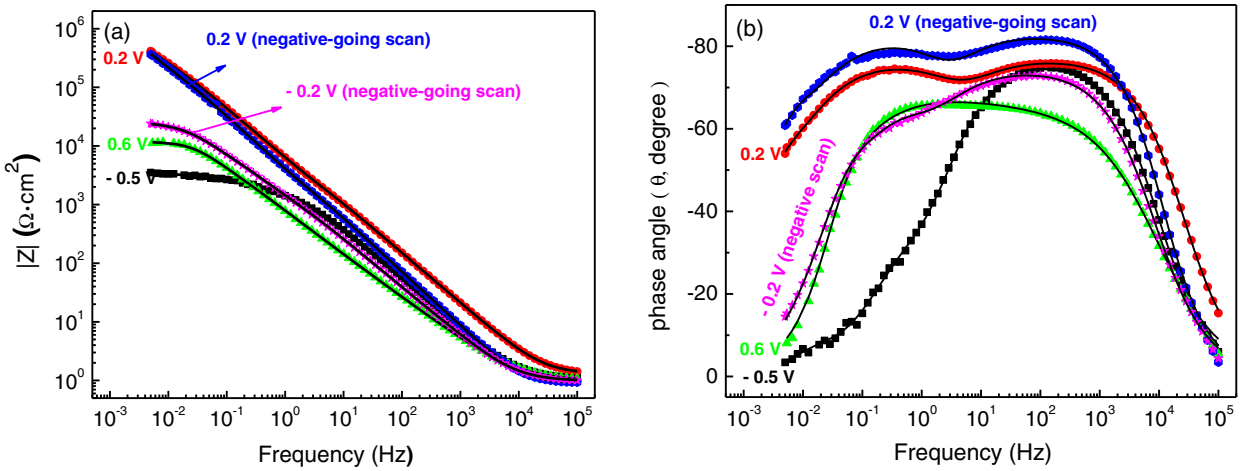

Figure 5. Impedance spectra (Bode plots) recorded on Alloy C-22 in oxygenated 5 M NaCl at 70°C after potentiostatic oxidation for 2 h at selected potentials applied on the positive-going and negative-going scans. The symbols are data points and the solid curves are fits of these spectra by the equivalent circuits shown in Figure 6.

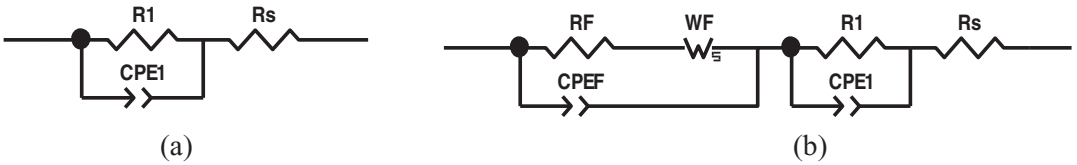

Figure 6. Electrical equivalent circuits used to fit impedance spectra recorded on Alloy C22 at 70°C in (a) potential regions 1 and 3 and (b) potential region 2. The circuits consist of a solution resistance (R_s), a charge transfer resistance (R_1) and constant phase element (CPE_1) combination, a film resistance (R_F) and constant phase element (CPE_F) combination, and a short-circuit Warburg element (W_F).

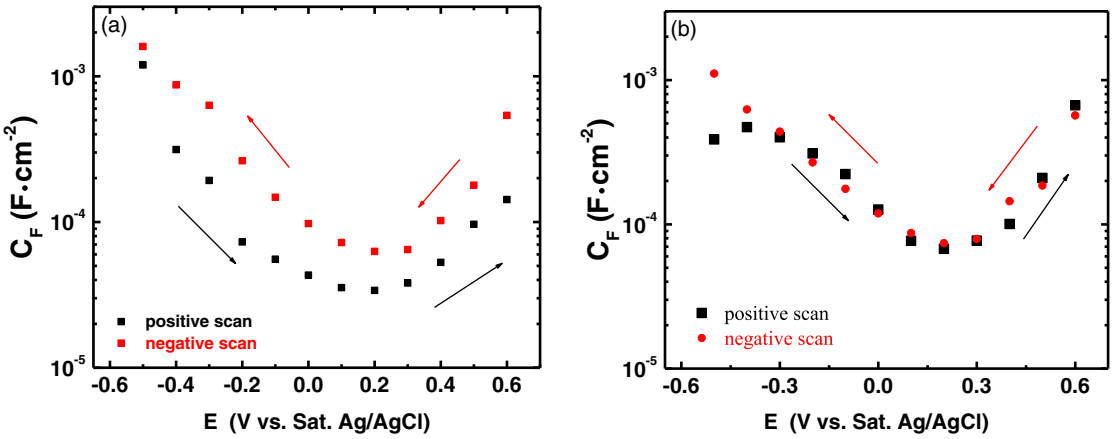

Figure 7. Variation of the film capacitances (C_F) obtained from fits to the spectra recorded on the positive and negative scans in both (a) deoxygenated and (b) oxygenated 5 M NaCl solutions at 70°C during a potentiostatic polarization experiment.

The fitted CPE exponents in our measurements, n, were >0.8 for spectra recorded at all applied potentials, except at the negative and the positive ends of the potential range recorded on the negative scan. In potential regions 1 and 2 the values of n are considerably lower, suggesting that other contributions, such as pseudo-diffusive impedance, could also contribute to the CPE behavior. As we have shown previously[1] in these regions the quality of the fit was markedly improved by including a Warburg impedance (W_F in Figure 6b). Its inclusion increased the values for the exponent n of the CPEs to > 0.85. This improvement indicates that transport processes within the defective oxide (potential region 1) and in the possibly porous surface Mo^{VI}/W^{VI} layer (potential region 3) play a role in the impedance response. This behavior has been discussed in more detail previously.[1]

On the assumption that the non-ideal capacitative behavior is attributable to distributed time-constants within the oxide film, the impedance of the CPE can be converted to yield a capacitance using the method described by Hsu and Mansfeld.[49] Figure 7 shows the capacitances (C_F) converted from the CPE_F that were obtained from fits to the spectra recorded on the positive and negative scans in both deoxygenated and oxygenated solutions. The resultant film capacitance values appear large for a regular oxide film, which may be due to the conversion, since it was claimed by Hirschorn et al.[50] that the Hsu and Mansfeld conversion could overestimate the effective capacitance. This issue will be discussed in a future article, and here the trends, instead of the absolute capacitance values, are the focus. The higher capacitances at negative and positive potentials could also be the consequence of the presence of a highly defective film at negative potentials and the presence of a surface layer containing high oxidation states of Mo and W, and possibly Cr, at positive potentials.

Figure 8 shows the corresponding resistance values, R_p, equal to the sum of the charge transfer (R_1) and passive film (R_F) resistances. The very rapid decreases in C_F (Figure 7) as the potential is increased (positive scan) and R_p (dominated by R_F for $E > -0.5$ V) increases (Figure 8) are the responses expected due to the growth of, and elimination of defects in, the passive film. In deoxygenated solution the capacitances measured on the negative scan are higher than on the positive scan, most likely an indication of the film degradation induced at positive potentials, which is not fully repaired on the negative scan. This discrepancy is not observed in oxygenated solutions. Whether this difference is significant is presently unclear.

Figure 8a compares the interfacial resistance, R_p, on the positive and negative scans in the deoxygenated solution. The plateau in R_p (−0.6 V to −0.4 V) followed by a further increase in R_p by one order of magnitude indicates that the establishment of passivity occurs in two stages. This increase in the interfacial resistance occurs over the potential range within which the O_2 reduction current (in oxygenated solution) on the positive scan decreases, Figures 2 and 3, confirming that this decrease is due to passivation of the surface. In the oxygenated solution, the resistance in this potential region is considerably lower, Figure 8b, reflecting the presence of an electron acceptor in the solution.

Since it is generally accepted that complete passivation is due to the formation of a Cr^{III} oxide-dominated barrier layer at the alloy/oxide interface, this sudden rise in R_p indicates that this layer only becomes

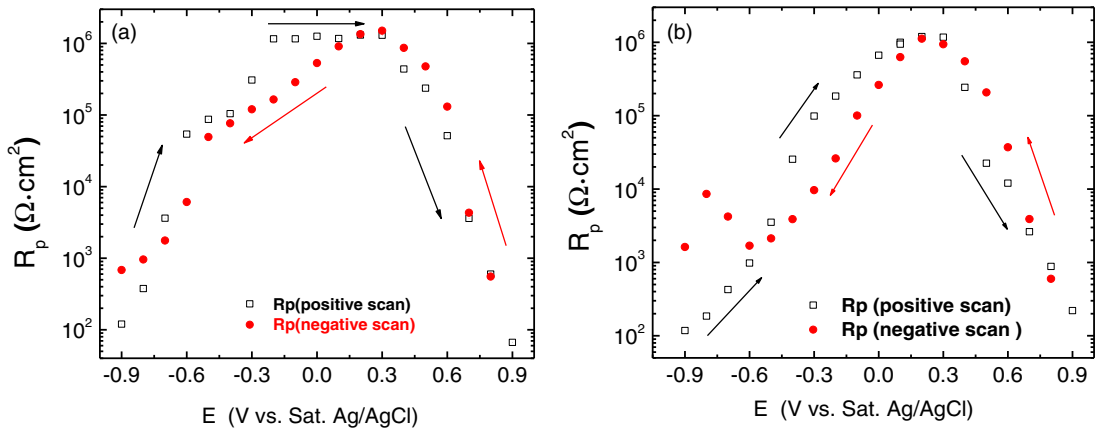

Figure 8. Interfacial resistance R_p (= R_1 + R_F) from impedance spectra recorded after potentiostatic oxidation for 2 h at various potentials on the positive and negative scans in 5 M NaCl solution at 70°C in (a) deoxygenated solution; and (b) oxygenated solution.

fully formed in this potential region. The specific processes within the film which lead to this improvement in passivity are presently unresolved. Since the oxidation of Cr is expected at very low potentials and its concentration in the barrier layer requires the segregation of Mo, and to a lesser degree W, to the outer regions of the film,[9,12,30,31] a possibility is that this improvement in passivity can be attributed to the oxidation of Mo leading to the segregation process.

The resistance measured in region 3 ($E > 0.3$ V) decreased rapidly as the potential increased on the positive scan, as expected due to the destruction of the Cr^{III} barrier layer. On the negative scan, R_p in region 3 was slightly larger than on the positive scan, consistent with the presence of a Mo^{VI}/W^{VI} layer which both thickened and spread as the potential was increased on the positive scan. As the potential was decreased, R_p decreased considerably over the potential range 0.1 V to −0.3 V confirming that the passivity induced on the positive scan, and destroyed by the excursion into region 3, had not been completely re-established at high potentials (0.4 V to 0.1 V) despite the high R_p values observed. As demonstrated in Figure 3, this allowed the reduction of O_2 to recommence, with the enhanced reduction current demonstrating that this reaction is catalyzed on the Mo^{VI}/W^{VI} surface states produced in region 3.

The temporary increase in R_p (for $E \leq -0.6$ V) in oxygenated solution coincides with the peak in the O_2 reduction current, confirming that the electrochemical reduction of these states leads to a suppression of O_2 reduction accounting for the decreased current for this reaction when the negative CV scans are reversed at −1.0 V, Figure 3. The progressive destruction of the passive film as the potential is increased in region 3 and the fact that it is not completely reformed on the subsequent negative scans, Figures 7 and 8, is confirmed by the need for a re-oxidation peak in the potential region −0.6 V to −0.3 V in the CVs, Figure 3, i.e., in the potential region immediately prior to the onset of complete passivation on the positive scan. As noted above this oxidation process could be due to the oxidation of Mo, leading to the re-formation of the Cr^{III} barrier layer as Mo^{III}/Mo^{IV} cations segregate to the outer regions of the passive film.[30]

Conclusions

Over the potential range investigated, three distinct regions of behavior have been identified: (i) region 1 at negative potentials at which the surface is covered with a highly defective oxide with a high concentration of anion vacancies; (ii) region 2 at intermediate potentials at which the surface is covered with a bilayer passive oxide comprising an inner Cr^{III}-dominated barrier layer with a $Mo^{III/IV}$ enriched outer layer; and (iii) region 3 at higher potentials at which the Cr^{III} barrier layer is degraded by anodic oxidation, and a film of Mo^{VI}/W^{VI} species accumulates on the surface.

Oxygen reduction can occur on the defective oxide in region 1 and appears to proceed via a combination of $2e^-$ and $4e^-$ reduction processes, but is completely suppressed in region 2. Once the passive film is formed, the O_2 reduction reaction cannot be revived unless the potential is temporarily increased into region 3. Such an excursion, leading to the destruction of the passive layer, revives the reaction, which is temporarily catalyzed on the transpassively created Mo^{VI}/W^{VI} surface species.

Once transpassively degraded, the passive film does not appear to be readily re-formed when the potential is returned to the passive region 2.

Acknowledgments

This project was funded by National Science and Engineering Research Council of Canada (NSERC). We are grateful to Haynes International, Kokomo, Indiana, for their donation of materials.

References

1. P. Jakupi, D. Zagidulin, J. J. Noël, and D. W. Shoesmith, *Electrochim. Acta*, **56**(17), 6251 (2011).
2. A. C. Lloyd, D. W. Shoesmith, N. S. McIntyre, and J. J. Noël, *J. Electrochem. Soc.*, **150**(4), B120 (2003).
3. A. C. Lloyd, J. J. Noël, N. S. McIntyre, and D. W. Shoesmith, *JOM*, **57**(1), 31 (2005).
4. D. D. MacDonald and A. Sun., *Electrochim. Acta*, **51**, 1767 (2006).
5. N. Priyantha, P. Jayaweera, D. D. Macdonald, and A. Sun, *J .Electroanal. Chem.*, **572**, 409 (2004).
6. M. Bojinov, P. Kinnunen, and G. Sundholm, *Corrosion*, **59** (2), 91 (2003).
7. M. Bojinov, A. Galtayries, P. Kinnunen, A. Machet, and P. Marcus, *Electrochim. Acta*, **52**, 7475 (2007).
8. R. M. Carranza and M.A.Rodriguez, *J. Electrochem. Soc.*, **158** (6), C221 (2011).
9. A. C. Lloyd, J. J. Noël, N. S. McIntyre, and D. W. Shoesmith, *Electrochim. Acta*, **49**(17–18), 3015 (2004).
10. J. J. Gray, B. S. El Dasher, and C. A. Orme, *Surf. Sci.*, **600**(12), 2488 (2006).
11. J. R. Hayes, A. Szmodis, K. L. Anderson, and C. A. Orme, *Corrosion 2004*, paper No. 04697, New Orleans, LA, NACE International.
12. C. R. Clayton and Y. C. Lu, *J. Electrochem. Soc.*, **133**(12), 2465 (1986).
13. J. J. Gray, J. R. Hayes, G. E. Gdowski, B. E. Viani, and C. A. Orme, *J. Electrochem. Soc.*, **153**(3), B61 (2006).
14. K. J. Evans, A. Yilmaz, S. D. Day, L. L. Wong, J. C. Estill, and R. B. Rebak, *JOM*, **57**(1), 56 (2005).
15. X. He and D. S. Dunn, *Corrosion*, **63**(2), 145 (2007).
16. K. J. King, J. C. Estill, M. L. Stuart, G. A. Hust, and R. B. Rebak, *Corrosion 2005*, paper No. 05607, Houston, TX, NACE International.
17. P. Jakupi, J. J. Noël, and D. W. Shoesmith, *Corr. Sci.*, **53**, 3122 (2011).
18. P. Jakupi, J. J. Noël F.Wang, and D. W. Shoesmith, *Corr. Sci.*, **53**, 1670 (2011).
19. P. Jakupi, J. J. Noël, and D. W. Shoesmith, *Corr. Sci.*, **54**, 260 (2012).
20. N. Ebrahimi, J. J. Noël, and D. W. Shoesmith M.Rodriguez, *Corr. Sci.*, **105**, 58 (2016).
21. N. Ebrahimi, P. Jakupi, J. J. Noël, and D. W. Shoesmith, *Corrosion*, **71**, 1441 (2015).
22. A. Davydov, K. V. Rybalka, L. A. Beketaeva, G. R. Engelhardt, P. Jayaweera, and D. D. Macdonald, *Corros. Sci.*, **47**(1), 195 (2005).
23. W. H. Hocking, J. S. Retteridge, and D. W. Shoesmith, Mechanism of the cathodic reduction of oxygen on UO_2 electrode, Atomic Energy of Canada Ltd. Report (September 1991) AECL-10402.
24. V. K. Ashok, *Electrochemistry of Metals and Semiconductors*, Marcel Dekker, New York (1973).
25. N. L. Bozec, C. Compère, M. L'Her, A. Laouenan, D. Costa, and P. Marcus, *Corros. Sci.*, **43**(4) 765 (2001).
26. V. Jovancicevic and J. O'M. Bockris, *J. Electrochem. Soc.*, **133**(9), 1797 (1986).
27. S. P. Rogers, D. F. Gervasio, and J. H. Payer, *ECS Trans.*, **3**(31), 431 (2007).
28. K. V. Rybalka, L. A. Beketaeva, and A. D. Davydov, *Corros. Sci.*, **54**, 161 (2012).
29. E. Asselin, A. Alfantazi, and S. Rogak, *J. Electrochem. Soc.*, **154**(4), C215 (2007).
30. D. Zagidulin, X. Zhang, J. Zhou, J. J. Noël, and D. W. Shoesmith, *Surf. Interface Anal.*, **45**, 1014 (2013).
31. X. Zhang, D. Zagidulin, and D. W. Shoesmith, *Electrochim. Acta*, **89**, 814 (2013).
32. X. Zhang and D. W. Shoesmith, *Corros. Sci.*, **76**, 424 (2013).
33. I. B. Butler, M. A. A. Schoonen, and D. T. Rickard, *Talanta*, **41**, 211 (1994).
34. E. Barsoukov and J. Macdonald, *Impedance spectroscopy: Theory, experiment, and applications*, Wiley, Hoboken (2005).
35. U. Retter and H. Lohse, *Electrochemical impedance spectroscopy*, in: F. Scholz (ed), Electroanalytical methods, Springer, Berlin, 2005, pp. 159.
36. E. Barsoukov and J. Macdonald, *Impedance spectroscopy. Theory, experiment, and applications*, Wiley, Hoboken, 2005.
37. M. Bojonov, T. Laitinen, K. Makela, T. Saario, and G. Sundholm, *J. Electroanal. Chem.*, **504**, 29 (2001).
38. B. S. Norgren, M. A. J. Somers, and J. H. W. Dewit, *Surf. Interface Anal.*, **21**, 378(1994).
39. D. S. Dunn, Y.-M. Pan, K. T. Chiang, L. Yang, G. A. Cragnolino, and X. He, *JOM*, **57**, 49 (2005).
40. B. Levich, *Acta Physicochim. U.R.S.S.*, **17**, 257 (1942).
41. K. Kawahara and C. Tanford, *J. Biol. Chem.*, **241**(13), 3228 (1966).
42. D. Dyrssen, H. Eskilsson, and C. Haraldsson, *J. Electroanal. Chem.*, **262**, 161 (1989).
43. D. R. Lide, *CRC Handbook of Chemistry and Physics*, 90th ed. 2009–2010, CRC press.
44. R. T. Ferrell and D. M. Himmelblau, *J. Chem. Eng. Data*, **12**(1), 111 (1967).
45. A. J. V. Store and L. J. J. Janssen, *Anal. Chim. Acta*, **279**, 213 (1993).
46. D. Tromans, *Ind. Eng. Chem. Res.*, **39**, 805 (2000).
47. G. L. Brug, A. L. G. van den, Eeden, M. Sluyters-Rehbach, and J. H. Sluyters, *J. Electroanal. Chem.*, **176**, 275 (1984).
48. B. Hirschorn, M. E. Orazem, B. Tribollet, V. Vivier, I. Frateur, and M. Musiani, *Electrochim. Acta*, **55**, 6218 (2010).
49. C. H. Hsu and F. Mansfeld, *Corrosion*, **57** (9), 747 (2001).
50. B. Hirschorn, M. E. Orazem, B. Tribollet, V. Vivier, I. Frateur, and M. Musiani, *J. Electrochem. Soc.*, **157**, C458 (2010).